Influence of Rotor Topologies and Cogging Torque Minimization Techniques in the Detection of Static Eccentricities in Axial-Flux Permanent-Magnet Machine

Oladapo Omotade Ogidi, *Member, IEEE*, Paul S. Barendse, *Member, IEEE*, and Mohamed Azeem Khan, *Senior Member, IEEE*

***Abstract*—In this paper, the effect of static eccentricity on current harmonics and torque ripple in an axial-flux permanent-magnet machine with fractional-slot concentrated winding is investigated. Cogging torque minimization techniques are also explored in the presence of the anomaly to better understand their sensitivity to the condition. Also, the impact of single-sided and double-sided rotor topologies on both current harmonics and torque ripple is examined. It is found that static eccentricities incite significant increases in the amplitudes of space and sub-harmonics in the single-sided topology, which may be mitigated by the cogging torque minimization techniques. The double-sided topology is tolerant to the presence of static eccentricities unlike the single-sided topology; this is due to the opposing effect of the resulting asymmetrical properties of the air gap. Finally, this paper establishes a detection technique for static eccentricities in single-sided axial-flux permanent-magnet machine whereby the cogging torque minimization techniques do not impair on them.**

***Index Terms*—Axial-flux permanent-magnet (AFPM) machine, current harmonics, fault detection, fractional-slots concentrated windings (FSCW), rotor topologies, static eccentricity, torque ripple.**

I. Introduction

THE axial-flux permanent-magnet (AFPM) machine is becoming increasingly popular, particularly in direct-drive wind turbine (WT) and electric vehicle (EV) applications [1]. Due to environmental and economic challenges caused by the burning of fossil fuels and its depleting reserve, respectively, both WT and EV are deemed fit as sustainable alternatives in power generation and transportation. Numerous topologies are associated with the AFPM machine, some of these have been identified in [2]–[6]. Key features in their design are the large aspect ratio (ratio of outer diameter to axial length) and rotor structural mass which accounts for half of the total active mass. These make them susceptible to static eccentricities (SE), which can impair their performance, cause structural imbalance, mechanical stress and strain on bearings [7]. The maximum allowable manufacturing tolerance for SE in permanent-magnet (PM) machines is 10%, above this, cases may be considered as faults [8], [9]. SE may also occur due to manufacturing imperfections such as unbalanced mass and bearing tolerance, or may be caused by shaft bow and bearing damage [10], [11], resulting in unbalanced magnetic pull, vibrations, winding loosening, insulation fretting, stator-rotor rub and damage [12], [[13]. The effects of SE on cogging torque are examined in [14]–[18]. In [19] and [20], a hybrid of finite-element analysis (FEA) and superposition method to investigate additional cogging torque harmonics resulting from misalignment of the rotor and stator caused by assembly and manufacturing tolerances in an AFPM machine is presented. Studies on reducing cogging torque by using certain techniques are investigated in [21]–[26]. However, the effects of these techniques on MMF harmonics under SE are not considered. In [8], the superposition of field functions was used to analytically evaluate the field and global quantities of the AFPM machine. FEA is then used to investigate the field shapes and identify the parameters. This approach helps us to analyze the effect of rotor dissymmetry on the circulation of current among winding parallel path. Though the technique gives insight into the behavior of the machine, it cannot detect faults in real time. In [27] and [28], the effects of static eccentricity on AFPM machines using FEA are studied. Results reveal unbalance in magnetic forces and torque. In [10], reduced magnitudes of induced electromotive force (EMF) on the stator coils adjacent to the region with increased air gap are observed. The results were verified experimentally but the detection methods are offline since individual stator coils need to be floating for measurement of back EMF. Noninvasive diagnostic techniques are identified in [11]–[13] and [29], phase current monitoring is identified as an alternative for condition-based maintenance due to lower cost and ease of measurement. Sideband frequencies are proposed as an index for eccentricity diagnosis but the prototype investigated is a radial-flux topology with integral winding configu-

Manuscript received February 17, 2016; revised June 15, 2016 and September 16, 2016; accepted September 30, 2016. Date of publication October 11, 2016; date of current version January 18, 2017. Paper 2016-EMC-0064.R2, presented at the 2015 IEEE Energy Conversion Congress and Exposition, Montreal, QC, Canada, Sep. 20–24, and approved for publication in the IEEE Transactions on Industry Applications by the Electric Machines Committee of the IEEE Industry Applications Society.

O. O. Ogidi is with Suzlon Energy Limited, Rostock 18057, Germany (e-mail: ogdola001@myuct.ac.za).

P. S. Barendse and M. A. Khan are with the Department of Electrical Engineering, University of Cape Town, Cape Town 7700, South Africa (e-mail: paul.barendse@uct.ac.za; azeem.khan@uct.ac.za).

Color versions of one or more of the figures in this paper are available online at http://ieeexplore.ieee.org.

Digital Object Identifier 10.1109/TIA.2016.2616320

ration [11]. The larger amplitudes of dynamic eccentricities are used to discriminate it from SE. However, some of the frequencies coincide with other rotor fault frequencies, such as shaft misalignment and broken magnets frequencies, etc. [12], [13].

In this paper, using FEA and experimental verification, the following are investigated.

1) The impact of cogging torque minimization techniques (CTMTs), namely magnet skewing and magnetic pole arc alternation, on current harmonics and torque ripple. Also, their effect on machine performance in the presence of SE is studied since they are widely applied in the design of PM machines.
2) The impact of rotor topologies, namely single-sided (SS) and double-sided (DS) topologies on torque ripple and current harmonics in the presence of SE.
3) Detection technique for SE in fractional-slot concentrated-windings (FSCW) AFPM machine using current analysis; space harmonics are examined alongside the sideband components.

The CTMTs and rotor topologies are analyzed in Section II. SE and the modeling technique are detailed in Sections III and IV, respectively. The results of the cases considered are discussed in detail in Section V.

II. Effect of the CTMTs and Rotor Topologies on Harmonics

The mathematical analysis of cogging and the effects of CTMTs are well documented in the literature [16]–[20]. Magnet skewing is a popular method of reducing cogging torque but due to manufacturing difficulty and high cost, alternating PM arc width is used as an alternative [16]. The alternating PM arc width technique is equivalent to the magnet skewing as it diminishes cogging torque harmonics using similar principles but the determination of an appropriate pole arc width for the alternate poles is difficult in design [16].

The two main rotor topologies are the DS and SS topologies [1], [5]; the DS topology is derived to overcome the increasing aspect ratio as the power rating in the SS topology increases [5]. In this section, the impact of CTMTs and rotor topologies on flux linkage ψ^v and winding factor $k^v{}_w$, respectively (where v is a harmonic order), is examined. This is because both flux linkage and winding factor are good indicators of MMF harmonic content.

A. Cogging Torque Minimization Techniques

The flux due to PMs which links all the windings gives the flux linkage for each phase under no load. Considering high harmonics, flux linkage per phase is described in (1), where $\hat{\psi}_{\rm PM}$ is the peak PM flux linkage of the vth harmonic and θ is the rotor position in electrical degrees

$$\psi_{\rm ph}\left(\theta\right) = \sum_{v}^{\infty} \hat{\psi}^v_{\rm PM} \sin v\theta. \tag{1}$$

Since skewing changes the relative position between the stator slots and rotor PMs across the circumference of an AFPM machine, the magnetic field distribution varies. Thus, taking into account the skewing effect, the flux linkage for each harmonic order due to the PMs is deduced in (2) under the following assumptions.

1) The origin of the general reference frame is taken to be at the center of the machine.
2) The circumferential variation of the saturation due to skewing is neglected.
3) Using the *xyz*-coordinate system in Fig. 1, the flux linking in (2) is over the active radius of the machine $-0.5D \leq z \leq 0.5D$

$$\psi^v\left(\theta\right) = \hat{\psi}^v_{\rm PM} \sin v\theta. \tag{2}$$

Thus, the vth harmonic of PM flux linking of a machine with skewing is described in (3), where $k_{\rm skv}$ is the skewing factor due to PMs for vth harmonic as described in (4) [32]. The harmonic components of the flux linkage may be reduced by $k_{\rm skv}$ using skewed or alternating PM pole, thus making flux density more sinusoidal in the air gap

$$\hat{\psi}^v_{\rm sk}\left(\theta, z\right) = k^v{}_{\rm sk} \hat{\psi}^v_{\rm PM} \sin v\theta \tag{3}$$

$$k^v{}_{\rm sk} = \frac{\sin\left(v \frac{s_{\rm sk}}{\tau_p} \frac{\pi}{2}\right)}{v \frac{s_{\rm sk}}{\tau_p} \frac{\pi}{2}} \tag{4}$$

where $s_{\rm sk}$ is the skewing pitch ratio and τ_p is the pole pitch.

B. Rotor Topologies

As a consequence of the dual air gap in the DS topology, it becomes amenable to multilayer (four layers) windings compared with double layer in the SS topology. Thus, by going from two to four layers, the synchronous winding factor is improved as a result of decrease in the distribution factor $k_{\rm dv}$ in (5) [30]–[32]. In a FSCW, $k_{\rm dv}$ cannot be simply defined; however, using voltage phasor $k_{\rm dv}$ is deduced in [30] and [31] for various layers and slot/pole combinations. For example, the winding factor in the double-layer winding of the prototype reduces from 0.067 to 0.0173 in the four layer windings for the fundamental harmonic component. Consequently, a combination of CTMTs with multilayer winding of the DS topology may result in larger reduction of $k^v{}_w$

$$k^v{}_w = k^v{}_p k^v{}_d k^v{}_{\rm sk}. \tag{5}$$

III. Modeling of SE in an AFPM Machine

A. Two-Dimensional Analytical

SE is a condition in which the axis of the rotor overlaps with its rotational axis but is deflected from that of the stator [8], [11]. The center line of the shaft is positioned at a constant offset from the stator, causing a time-invariant nonuniform air gap. The phenomenon of SE in AFPM machines is more penetrating than in the radial-flux type because it is inherently a 3-D and complex geometry; as such the physical modeling of SE is difficult. However, a 2-D plane in Fig. 1 is used in this paper to reduce the scale of the geometry and to provide bases for precise replication of the fault in FEA and experimentation. The machines under investigation are the surface-mounted PM, iron

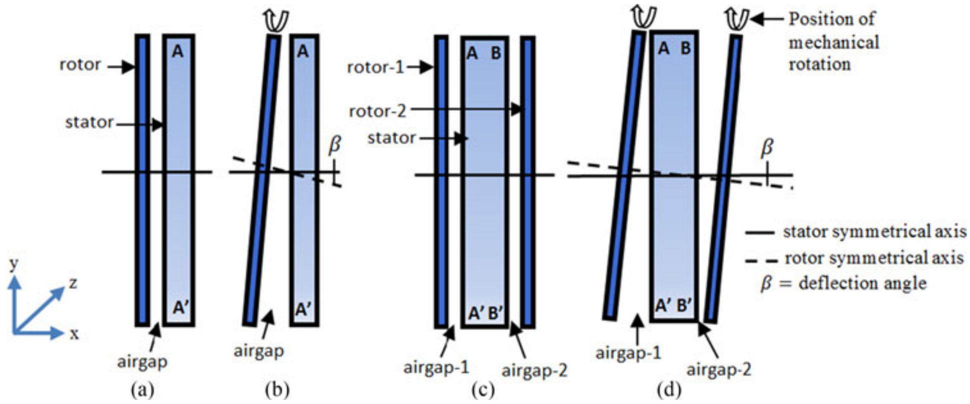

Fig. 1. AFPM machine in 2-D plane: (a) and (b) SS topology. (c) and (d) DS topology.

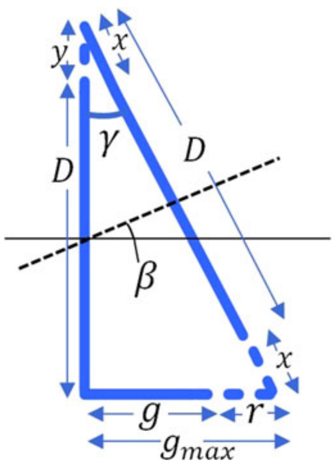

Fig. 2. Cross section of the asymmetric air gap.

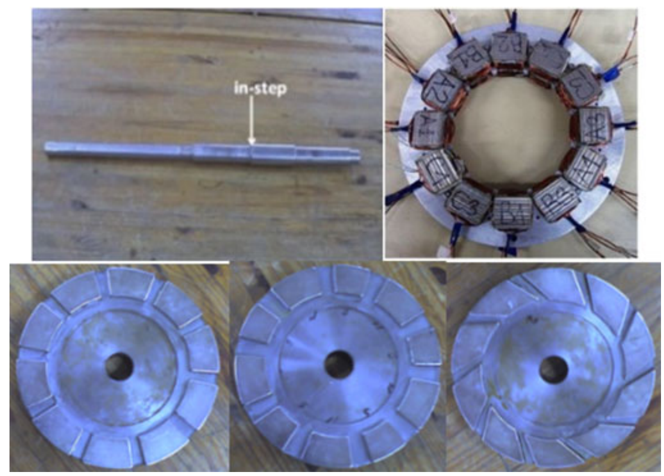

Fig. 3. PM configurations on the rotor discs; equal PM pole, alternating PM pole and skewed PM pole, respectively (bottom), the rotor shaft (top left), and FSCW on stator core (top right).

core stator, and SS and DS topologies in Fig. 1. The SS topology has a rotor disc and single air gap, while the DS topology has two air gaps and two rotor discs which rest on a common shaft. The healthy state is shown for SS and DS in Fig. 1(a) and (c), respectively, the air-gap length g is uniform along the axial direction (x-coordinate) and around the circumference (y-coordinate) of the stator. Here, the symmetrical axis of the rotor coincides with that of the stator, irrespective of the mechanical rotation. However, in the event of occurrence of SE, the rotor shaft experiences a deflection and the symmetry of the rotor deviates from the stator's by an angle β and the air gap varies in axial length from small to large around the circumference of the stator. This variation is fixed in space, that is, it is independent of the position of mechanical rotation for SS and DS. For this reason, permeance will vary axially across the machine circumference from maximum to minimum in the regions of minimum to maximum air gap, respectively. In the DS topology [see Fig. 1(c) and (d)], the deflection of one rotor is conversely reflected on the other in equal proportion. This causes the minimum reluctance seen by a stator face to experience a corresponding maximum reluctance on the opposite face since the rotor discs rest on a common shaft.

Fig. 2 (not drawn to scale) illustrates the worst possible scenario of the resulting asymmetric air gap due to SE. Here, mechanical clearance ceases to exist and the rotor disc starts to make contact with the stator. Thus, (6)–(8) are derived from the geometry, where D is the diameter of the rotor disc, and γ and $g_{\max}$ are the resulting deflection angle and air-gap length, respectively. The increase in g is a consequence of the deflection length r which is directly proportional to β, with the greatest possible limit reached in (6) and (7). Therefore, irrespective of the diameter of an AFPM machine, its deflection length from its axis is within the limits of the air gap, i.e., the variation in air-gap length caused by SE is $g_{\min} \geq 0 \leq 2g \geq g_{\max}$ and the deflection length $r \leq g$. It can be measured in (9) as a percentage ratio of the deflection length to the length of the ideal air gap and the effective length of air gap caused by SE is expressed in (10), where φ is the time-invariant spatial position. In practice, although $4g^2 \ll (D+x)^2$ in (8), when $\gamma \gg 0$, a significant SE factor given in (9) will result. Furthermore, since $0 < x$ and $0 < y$ in Fig. 3, a leakage flux will occur. These effects of SE on the magnetic field are better accounted for in FE computation using this 2-D model in 3-D FEA

$$g_{\min} = g - r = 0 \tag{6}$$

$$g_{\max} = g + r = 2g \tag{7}$$

TABLE I
MACHINE PARAMETERS

Parameters	Value
Rated Power	450 W
Nominal Speed	600 r/min
Nominal Torque	7 N·m
Number of Turns/Phase	20
Pole Pair	5
Number of slots	12
Outer Diameter	180 mm
Axial Length	27 mm
Length of air gap	1.5 mm
Inertia	0.048 $\text{Kg} \cdot \text{m}^2$
Stator Resistance (*L–N*)	0.40 Ω
Stator Inductance (*L–N*)	7.4 mH

$$\frac{4g}{(D+x)} = \sin\gamma \tag{8}$$

$$\epsilon_s = \frac{r}{g} \times 100\% \tag{9}$$

$$g_e(\varphi) = g(1 \pm \epsilon_s). \tag{10}$$

B. Three-Dimensional FEA

The basis of any reliable fault diagnosis method for electric machines is precise performance analysis under both healthy and faulty conditions. Modeling of the fault is imperative in understanding and diagnosing the condition. Thus, approaches that consider all effective characteristics of machines, such as FEA, are reliable for investigating faulty machines [33]. The major advantage of the FEA is that physical geometries can be modeled mathematically and numerical techniques can be employed to give precise electromagnetic solutions. Although at present, commercial 2-D/3-D FEA software packages are primarily not designed for fault investigations, their effective application for fault analysis can be skillfully achieved. Cedrat's Flux is the commercial FEA software used to analyze the AFPM machine topologies under both healthy and faulty scenarios. Using the parameters of the prototype in Table I, SE is replicated by offsetting the geometrical coordinates of the stator with respect to the rotor to achieve the desired degree of SE as described in Section II-A. The FEA takes into account significant practical parameters, such as saturation, leakage flux, finite permeance of magnetic materials, teeth, and slotting effects. For a healthy machine, the FEA could be done by modeling a part of the geometry and applying periodicity since electrical machines have symmetrical characteristics. However, such simplification cannot be used in the case of SE since it alters the symmetrical properties of the machine. Thus, full geometrical modeling is performed using 3-D FEA since the AFPM machine is inherently a 3-D geometry.

IV. Prototypes, Fault Implementation, and Measurements Scheme

A. Prototypes

The surface-mounted PM machine in both DS and SS topologies are investigated. The three magnet configurations on the rotor disc of the prototypes are shown in Fig. 3. They are equal PM pole, alternating PM pole, and skewed PM poles. The fitting skew angle and magnetic pole width for both skewed and alternating PM pole, respectively, both used as configurations to minimize cogging torque are derived for the prototype in [23]. The pole-arc ratio and skewing angle per slot pitch is given in Table II. The full-design details are given in [23]. The prototypes are modular designs having their number of poles p and slots Q differ by 2, i.e., $Q \pm p = 2$; thus, it employs the FSCW configuration, a winding type inherently rich in current harmonics because of the slots per pole per phase $q < 1$ [25], [26], [30]. However, the FSCW configuration has advantages of short-end regions, ease of manufacturing, large self-inductance, low fault probability of coil–coil short circuit, high-flux weakening capacity, high efficiency, high power, and torque density.

TABLE II
MAGNET CONFIGURATIONS ON THE PROTOTYPES

	Conventional Technique	CTMTs	
Rotor Topologies	Equal PM Pole	Skewed PM Pole	Alternate PM Pole
SS	0.80	$6^\circ\ \alpha_{\text{skew}}$	0.61–0.80
DS	0.80	$6^\circ \alpha_{\text{skew}}$	0.61–0.80

B. Fault Implementation

The axial magnetic force and pressure between the rotor and stator is very high; thus, restraint of the rotor inclines due to SE as seen in Fig. 1 is difficult. To practically implement the fault, the stator was housed on a flange which was fitted onto a rigid external frame. The flange is adjustable and its position on the external frame can be varied to obtain SE by displacing the stator axis from the rotor axis at an angular offset (illustrated in Fig. 1) corresponding to the desired degree of SE. The rotor shaft was also designed with an in step to rest the rotor disc and prevent the rotor from moving toward the stator (both shaft and rotor discs are shown in Fig. 3). A fillet gauge was used to measure the resulting air-gap variation to ensure accuracy. The rotor structure was not altered; thus, the method eliminated the possibility of straining the bearing and inducing other faults during experimentation. The test rig developed in [34] was used for the experimentation, data acquisition, and analysis.

C. Measurements Scheme

Several methods of measuring cogging torque and torque ripple in PM machines have been identified in [23], [35], and [36]. A simple inexpensive method based on measuring the reaction torque on the stator is proposed in [35]. It makes use of a balancing beam which is frictionless, but may be a time-consuming process for multiple measurement scenarios. In [36], the use of a torque sensor is proposed, but to ensure accurate torque ripple measurement, mechanical dynamics is considered. In particular, the transfer function between the motor torque and measured torque should be time and frequency independent over the experimental operating range. The torque sensor should not measure inertial and bearing loads, otherwise the torque ripple created by the motor may be amplified before it is measured.

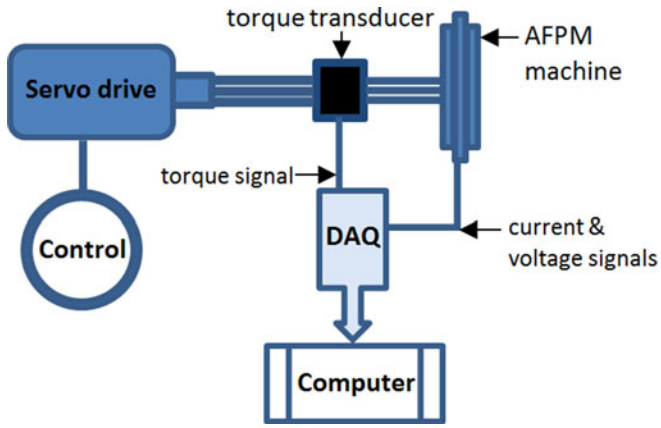

Fig. 4. Architecture of the experimental setup.

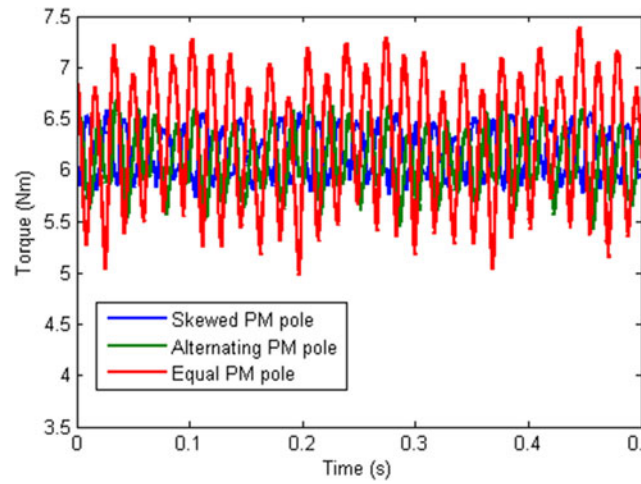

Fig. 5. Experimental measurement of the impact of the various CTMTs on torque.

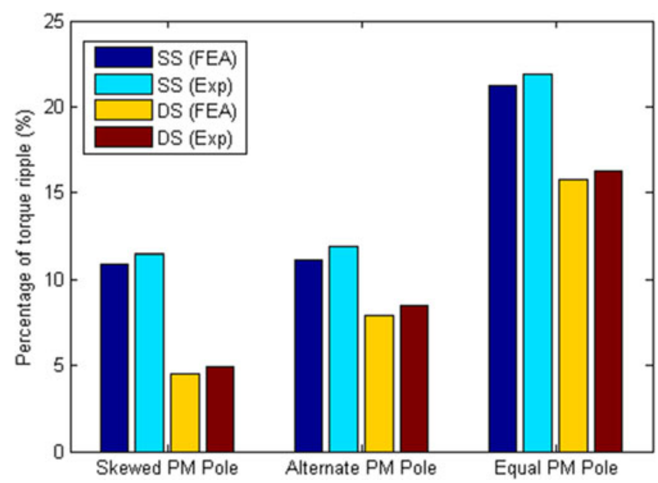

Fig. 6. Influence of rotor topologies on torque ripple.

In this paper, a calibrated 10-N·m DR-2112 brushless in-line torque transducer by Lorenz–Messtechnik [37] is selected for torque measurements. It can measure the maximum load with sufficient accuracy to capture torque ripple precisely. The accuracy class of the transducer is 0.1%, which is sufficient to measure low cogging torque values of the AFPM machine. To mitigate the effect of inertial loads, radial and axial reaction loads from the bearings on the torque readings, the transducer was connected to the servo drive and the AFPM machine by means of rigid couplings on both sides. A schematic representation of the test rig is shown in Fig. 4, and the measuring components are given in [34]. For the prototype investigated, based on (11) [17], there are five cogging cycles per slot pitch. Thus, for the cogging torque measurement, the speed of the servo drive (with a step resolution of 0.036°) was set to 0.0166 r/s, which corresponds to 6 °mech/s. This low speed ensured that the cogging cycles can be captured with an adequate resolution over each slot pitch. Besides the influence of inertial loads and reaction forces from the bearings, the measurement procedure using the values of a shaft torque is also predisposed to pulsating torque of the servo drive. It's peak value was confirmed to be less than 0.02 N·m and was considered in the cogging torque calculations. The pulsating torque of the servo drive was measured by replacing the stator of the AFPM machine with a nonferromagnetic dummy stator made of Perspex [23]. Current and voltage signals were also captured and the processing of all signals were done using a computer and NI LabVIEW interface

$$N_p = \frac{2p}{HCF\ \{Q,\ \ 2p\}} \tag{11}$$

where N_p is the number of cogging cycles and Q and $2p$ are number of slots and poles, respectively.

V. Evaluation of Electromagnetic and Electrical Quantities

The effect of SE on machine performance is determined by evaluating electrical and electromagnetic quantities. Using the Fourier transform and power spectrum density, the harmonics present in the line current of the machine are extracted for both healthy and SE scenarios under various load conditions and at different speeds in the *abc* reference frame. Inductance, torque, and flux density were computed from FEA. Current harmonics and also torque were obtained from experimentation to quantify the performance of the various rotor topologies and CTMTs. Since skewing decreases the rms value of the EMF fundamental wave as a result of reduced winding factor, the current and torque ratings are kept the same for both topologies and the three magnet configurations to provide a common template for the investigation.

A. Torque Ripple

1) Impact of CTMTs and Rotor Topologies on Torque Ripple Under Healthy Conditions: As deduced from experimental measurements, the effect of the various CTMTs on load torque is shown in Fig. 5–7. The torque response is unidirectional and has both constant and periodic components. The periodic component is a function of time, superimposed on the offset and it is the cause of the pulsation. Results are obtained using (12), (13) [38], where $T_{\rm av}$ is the average torque, $T_{\rm cogg}$ is the cogging torque, T_r is the total torque ripple, and $T_{\rm MMF}$ is the ripple due to MMF harmonics. At rated torque,

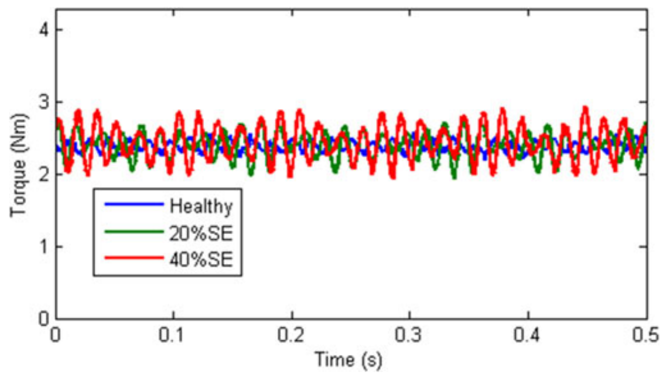

Fig. 7. Experimental measurement of torque pulsation under healthy and SE conditions in the SS topology.

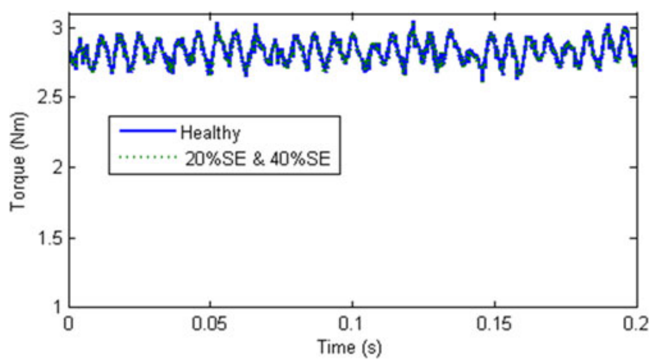

Fig. 8. Experimental measurement of torque pulsation under healthy and SE conditions in the DS topology.

the two CTMTs effectively reduced T_{MMF} in the equal PM pole configuration as seen in Fig. 6 from 21.5% to 11.5% in the alternate PM pole and 11% in the skewed PM

$$T_r(\propto) = \frac{T_{\max} - T_{\min}}{T_{\mathrm{av}}} \tag{12}$$

$$T_{\mathrm{MMF}} = T_r(\propto) - T_{\mathrm{cogg}} \tag{13}$$

pole configuration in the SS topology. In the DS topology, the torque ripples obtained are 16%, 8.2%, and 4.8% for the equal PM pole, alternate PM pole, and skewed PM pole configuration, respectively. The DS topology is more effective at reducing torque ripples due to MMF harmonics than the SS topology in combination with the CTMTs. The current harmonic components responsible for this are later examined in this section.

2) Impact of CTMTs and Rotor Topologies on Torque Ripple Under SE Condition: The torque response for the SS topologies using the skewed PM pole is shown in Fig. 7. In the presence of SE, T_{MMF} in the SS topology increased with the degree of SE for all three magnet configurations. The CTMTs produced significantly lower T_{MMF} than the equal PM pole configuration under SE.

In the DS topology, no ripple effect due to SE is manifested in the torque response, as shown in Fig. 8. The inductances have been computed in FEA to closely examine the effect. Fig. 9 shows the stator unsaturated inductances associated with the coils in the rotor position with minimum air-gap length for the SS topology. Since the air-gap length varies around the stator circumference, the inductances of the coils in all three phases vary. It is evident that the inductances increase with smaller length of air gap; however, in the DS topology in Fig. 10, no change in an inductance is evident for the same magnetic path. This phenomenon is better clarified in Fig. 11 showing the FEA plot of the normal component of flux density B_n using the center of the symmetric air gap as reference. Here, B_n in air gap-1 is conversely reflected in air gap-2 in the DS topology (indicated by the dotted circle for 120$^{\mathrm{o}}$ mech. position). The coils A and A' in Fig. 1(c) and (d) see minimum and maximum flux linkage, respectively, and the ensuing inductance from the pair remained unaffected. Thus, the DS topology is electromagnetically balanced under eccentricities. Variable air-gap permeance, which results from eccentricities, does not impair on the perfor-

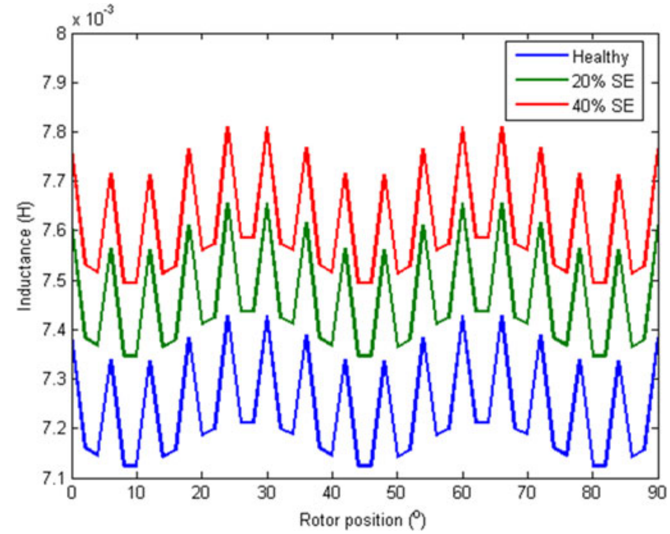

Fig. 9. FEA result of inductance of magnetic path across rotor position with minimum air-gap length in a SS topology.

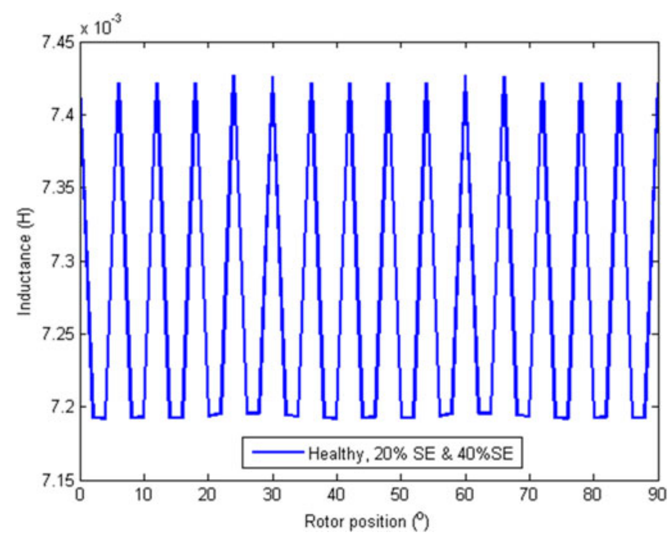

Fig. 10. FEA result of inductance of magnetic path across rotor position with minimum air-gap length in a DS topology.

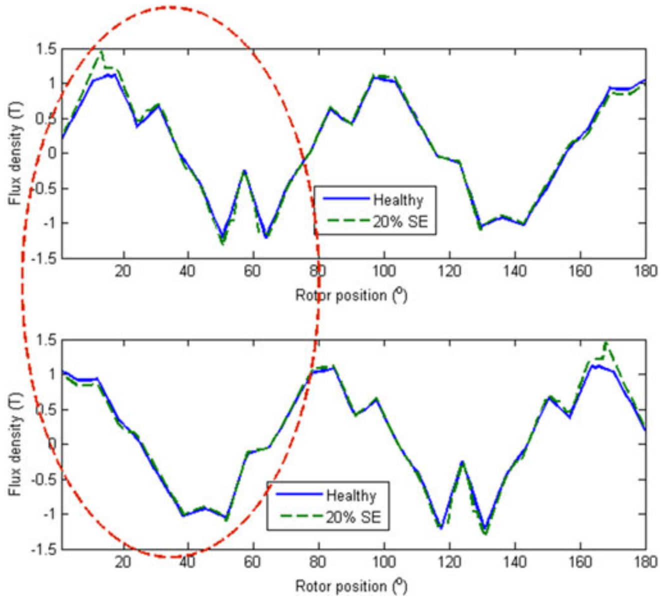

Fig. 11. Normal component of the magnetic flux density.

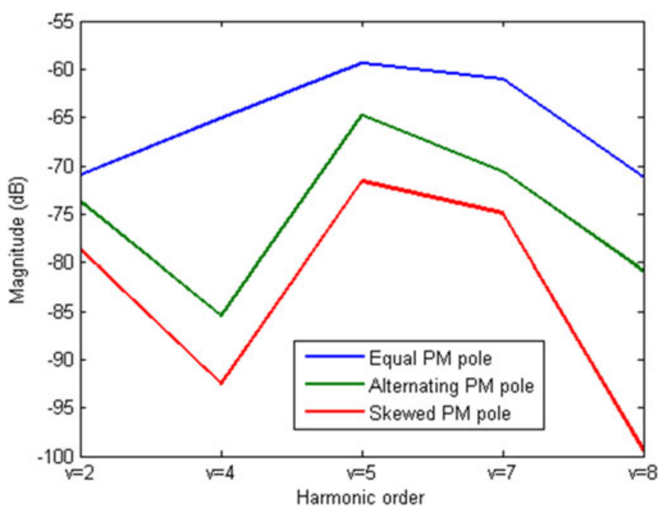

Fig. 12. Impact of the various CTMTs on v.

mance of the DS topology. This magnetic field behavior is the same for all the three magnet configurations in Table II.

B. Current Harmonics

1) Impact of CTMTs on Space Harmonics Under Healthy Condition: Before identifying incited current harmonics under faulty mode, an analysis of the current harmonics in the healthy machine is necessary. In the FSCW configuration, the coils are spatially displaced by a limited number of slots under a high number of pole pairs (i.e., $q < 1$) in a medium of nonsinusoidal air-gap flux density distribution. Thus, space harmonics are induced in the voltages. This causes the windings to operate at current linkage harmonics defined by (14) [23], [24], where $m = 3$ and $k = 0, 1, 2 \ldots$, yielding $v = 1, -2, +4, \ldots$; where the sign is indicative of the direction of rotation of the

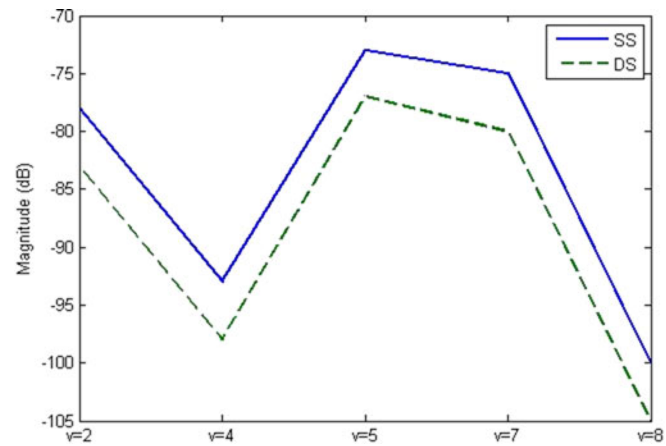

Fig. 13. Impact of the DS topology on v.

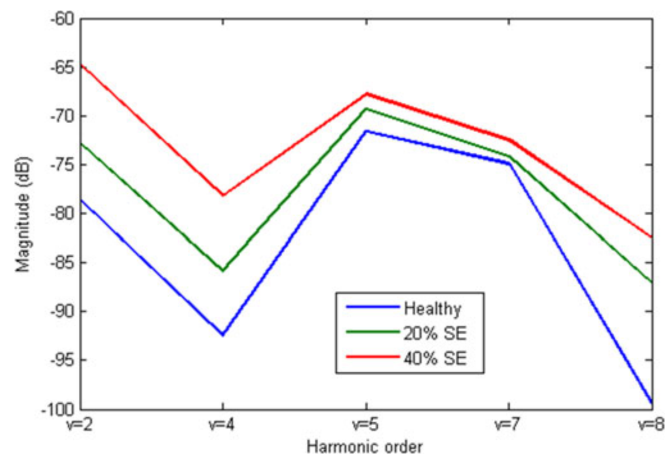

Fig. 14. Effect of SE on v.

harmonics based on the rotating field theory

$$v = 1 \pm km. \tag{14}$$

These space harmonics, which are inherently present, are of particularly interest in PM machines with concentrated winding because they may cause additional rotor eddy current losses [23]. In Fig. 12, the influence of the CTMTs on v is obtained. It shows that the CTMTs effectively reduce their magnitudes since they make flux density more sinusoidal, thereby inducing a more sinusoidal back EMF, and, consequently, leading to reduced current linkage harmonics. The reduction in MMF harmonics is desirable because they are the main source of torque ripple when PM machines operate under load. Notice that the even-order harmonics are lower in magnitudes than the odd-order harmonics since symmetry is maintained around the poles.

2) Impact of Rotor Topologies on Space Harmonics Under Healthy Condition: The amplitudes of v are reduced by an average of 5% in the DS topology, relative to the SS topology as shown in Fig. 13. Accordingly in Fig. 6, the lower T_{MMF} is derived from the torque response of the DS topology compared with the SS topology. The decrease in amplitude is a result of the multilayer winding in the DS topology, leading to

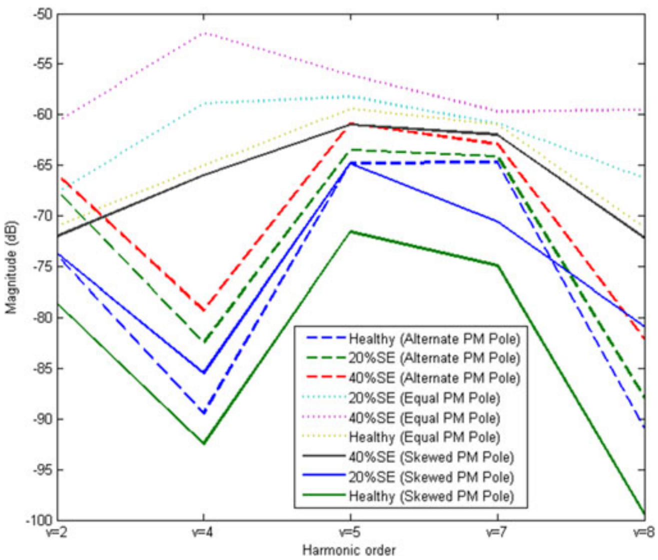

Fig. 15. Impact of the CTMTs on v under SE.

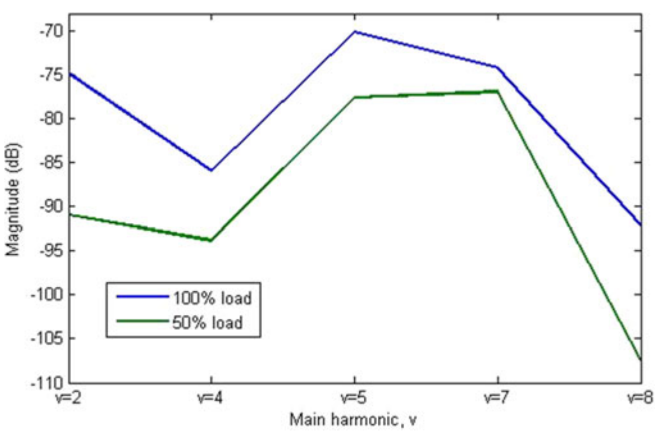

Fig. 16. Effect of load variations on v.

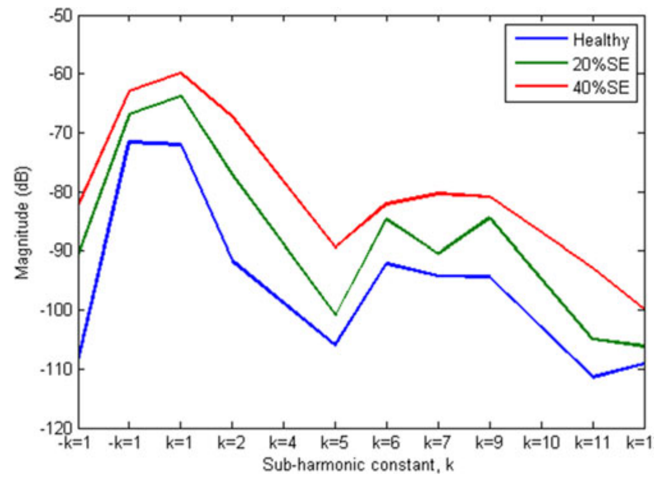

Fig. 17. Effect of SE on frequency components with harmonic constant k.

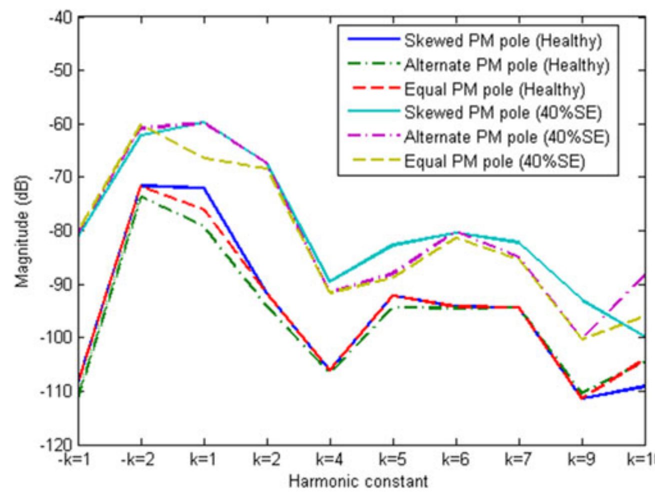

Fig. 18. Effect of SE on frequency components with harmonic constant k.

a slightly lower distribution factor in (10). The winding factor in the double-layer winding reduces from 0.067 to 0.0173 in the multiple layer windings for $v = 1$. Similarly, the winding factor when $v = 2,\ 4,\ 5,\ 7,\ 8$ in the double-layer configuration reduces from 0.933 to 0.9012 in the multiple layer winding.

3) Impact of Rotor Topologies and CTMTs on Space Harmonics Under SE Conditions: Fig. 14 shows the effect of SE on v using the alternate PM pole in the SS topology. The amplitudes are significantly affected by SE with the even-order harmonics being largely more incited than the odd harmonics since the space-variant air-gap permeance characteristics given in (13) leads to asymmetric distortion of the MMF wave over a pole pitch, where the coils are displaced by a limited number of slots. Consequently, the load torque in Fig. 8 is insusceptible to SE. Furthermore, the impact of the CTMTs on v under SE in the SS topology is revealed in Fig. 15, where all the three PM configurations are compared. The CTMTs considerably diminishes the amplitudes of v even in the presence of SE, but the amplitudes of v are unchanged in the DS topology under SE irrespective of the magnet configurations employed.

The magnitudes of v are clearly indicative of SE in the SS topology but they may not suffice as indices for fault detection since they are largely dependent on the CTMTs employed and load variations are impactful on them as seen in Fig. 16. Therefore, the subharmonics in the line current are explored for fault detection.

4) Subharmonics Under SE Condition, the Impact of CTMTs and Rotor Topologies: The amplitudes of the frequencies f_{SE} in (15), where f is the fundamental frequency of the line current, p is the number of pole pairs, and $k = 1,\ 2,\ 3\ldots$ are proposed as indices for diagnosis of SE in radial-flux PM machines with distributed windings [11]. They are sidebands of the fundamental component. In the DS topology of the prototypes investigated, the amplitudes of the sidebands in (15) are not affected under SE conditions with all three magnet configurations. However, in the SS topology, the sidebands significantly increased in amplitudes; the fault frequencies in (15) are found to be equally

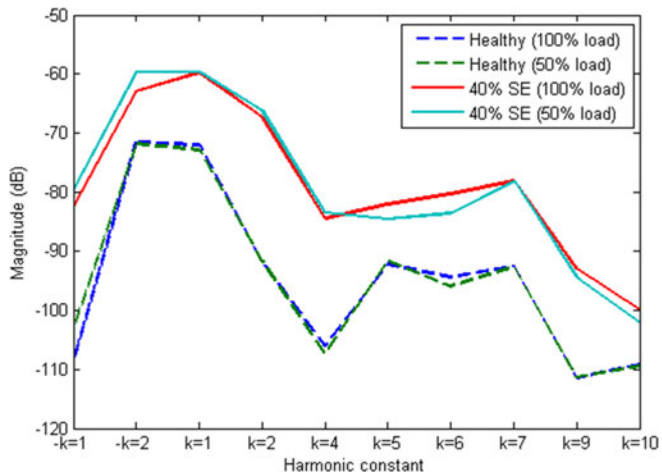

Fig. 19. Effect of load variations on frequency components with harmonic constant k.

valid for AFPM machines in the SS topology, as shown in Fig. 17.

Unlike the space harmonics, the subharmonics are not significantly affected by the CTMTs under healthy and SE conditions. The amplitudes are shown in Fig. 18. In addition, in Fig. 19, load variations are found to have no considerable impact on the amplitudes, thereby making (15) a robust detection technique. However, some components in (14) and (15) overlap, when v is an even-order harmonic and $k = 3, 8, 13\ldots$, respectively. The overlapping frequencies are, thus, excluded in the detection technique and trending derived in Fig. 15 since v varies significantly in amplitudes due to load changes

$$f_{\mathrm{SE}} = f\left(1 \pm \frac{2k-1}{p}\right). \tag{15}$$

VI. Conclusion

Space harmonics are significantly reduced using CTMTs and in the DS topology under healthy condition as a result of reduced flux linkage harmonics and winding factor, respectively. However, unlike the space harmonics, the subharmonics are not affected by the CTMTs or in the DS topology. Under SE conditions, increase in amplitudes of space and subharmonics are evident in the SS topology but not in the DS topology. This is effective for both CTMTs investigated. The immunity of the DS topology is due to the opposing effect of the asymmetrical properties of its two air gap. Thus, the DS topology is a more robust topology. It can correct the effects of rotor dissymmetry as a result of manufacturing imperfections or SE faults, while the CTMTs can mitigate the impact of SE in the SS topology. The technique for fault detection of SE in radial-flux PM machines with distributed windings as established in the literature is also applicable for the SS topology of the AFPM machine with concentrated windings if the frequency components which coincide with even-order space harmonics are not taken into account. The detection technique is robust against load variations and the CTMTs.

References

[1] F. Giulii Capponi, G. De Donato, and F. Caricchi, "Recent advances in axial-flux permanent-magnet machine technology," *IEEE Trans. Ind. Appl.*, vol. 48, no. 6, pp. 2190–2205, Nov./Dec. 2012.

[2] Y. Okumura, M. Sanada, S. Morimoto, and Y. Inoue, "Study of characteristics of various structures in axial-gap PM motors," in *Proc. 2012 15th Int. Conf. Electr. Mach. Syst.*, Oct. 21—24, 2012, pp. 1–6.

[3] Y. Chen, P. Pillay, and A. Khan, "PM wind generator topologies," *IEEE Trans. Ind. Appl.*, vol. 41, no. 6, pp. 1619–1626, Nov./Dec. 2005.

[4] M. J. Kamper, R.-J. Wang, and F. G. Rossouw, "Analysis and performance of axial flux permanent-magnet machine with air-cored nonoverlapping concentrated stator windings," *IEEE Trans. Ind. Appl.*, vol. 44, no. 5, pp. 1495–1504, Sep./Oct. 2008.

[5] J. F. Gieras, R. J. Wang, and M. J. Kamper, *Axial Flux Permanent Magnet Brushless Machines*. Dordrecht, The Netherlands: Kluwer, 2004.

[6] J. Pippuri, A. Manninen, J. Keranen, and K. Tammi, "Torque density of radial, axial and transverse flux permanent magnet machine topologies," *IEEE Trans. Magn.*, vol. 49, no. 5, pp. 2339–2342, May 2013.

[7] D. N. Mbidi, K. Van der Westhuizen, R. Wang, M. J. Kamper, and J. Blom, "Mechanical design considerations of a double stage axial-flux PM machine," in *Proc. 2000 Conf. Rec. IEEE Ind. Appl. Conf.*, 2000, pp. 198–201.

[8] A. Di Gerlando, G. M. Foglia, M. F. Iacchetti, and R. Perini, "Evaluation of manufacturing dissymmetry effects in axial flux permanent-magnet machines: Analysis method based on field functions," *IEEE Trans. Magn.*, vol. 48, no. 6, pp. 1995–2008, Jun. 2012.

[9] M. Valavi, A. Nysveen, and R. Nilssen, "Magnetic forces and vibration in permanent magnet machines with non-overlapping concentrated windings: A review," in *Proc. 2012 IEEE Int. Conf. Ind. Technol.*, Mar. 19—21, 2012, pp. 977–984.

[10] S. M. Mirimani, A. Vahedi, and F. Marignetti, "Effect of inclined static eccentricity fault in single stator–single rotor axial flux permanent magnet machines," *IEEE Trans. Magn.*, vol. 48, no. 1, pp. 143–149, Jan. 2012.

[11] B. M. Ebrahimi, J. Faiz, and M. J. Roshtkhari, "Static-, dynamic-, and mixed-eccentricity fault diagnoses in permanent-magnet synchronous motors," *IEEE Trans. Ind. Electron.*, vol. 56, no. 11, pp. 4727–4739, Nov. 2010.

[12] W. le Roux, R. G. Harley, and T. G. Habetler, "Detecting rotor faults in low power permanent magnet synchronous machines," *IEEE Trans. Power Electron.*, vol. 22, no. 1, pp. 322–328, Jan. 2007.

[13] Y. Duan and H. Toliyat, "A review of condition monitoring and fault diagnosis for permanent magnet machines," in *Proc. 2012 IEEE Power Energy Soc. Gen. Meet.*, Jul. 22—26, 2012, pp. 1–4.

[14] Z. Q. Zhu, L. J. Wu, and M. L. Mohd Jamil, "Influence of pole and slot number combinations on cogging torque in permanent-magnet machines with static and rotating eccentricities," *IEEE Trans. Ind. Appl.*, vol. 50, no. 5, pp. 3265–3277, Sep./Oct. 2014.

[15] S. Jagasics, "Comprehensive analysis on the effect of static air gap eccentricity on cogging torque," in *Proc. 2010 IEEE 19th Int. Workshop Robot. Alpe-Adria-Danube Region*, Jun. 24—26, 2010, pp. 447–449.

[16] S. Afsari kashani, H. Heydari, and B. Dianati, "Cogging torque mitigation in axial flux magnetic gear system based on skew effects using an improved quasi 3-D analytical method," *IEEE Trans. Magn.*, vol. 51, no. 9, Sep./Oct. 2015, Art. no. 7403111.

[17] N. Bianchi and S. Bolognani, "Design techniques for reducing the cogging torque in surface-mounted PM motors," *IEEE Trans. Ind. Appl.*, vol. 38, no. 5, pp. 1259–1265, Sep./Oct. 2002.

[18] F. Caricchi, F. G. Capponi, F. Crescimbini, and L. Solero, "Experimental study on reducing cogging torque and no-load power loss in axial-flux permanent-magnet machines with slotted winding," *IEEE Trans. Ind. Appl.*, vol. 40, no. 4, pp. 1066–1075, Jul./Aug. 2004

[19] M. Thiele, G. Heins, and D. Patterson, "Identifying manufacturing induced rotor and stator misalignment in brushless permanent magnet motors," in *Proc. 2014 Int. Conf. Electr. Mach.*, Berlin, Germany, 2014, pp. 2728–2733.

[20] M. Thiele and G. Heins, "Computationally efficient method for identifying manufacturing induced rotor and stator misalignment in permanent magnet brushless machines," *IEEE Trans. Ind. Appl.*, vol. 52, no. 4, pp. 3033–3040, Jul./Aug. 2016.

[21] C. Bianchini, F. Immovilli, E. Lorenzani, A. Bellini, and M. Davoli, "Review of design solutions for internal permanent-magnet machines cogging torque reduction," *IEEE Trans. Magn.*, vol. 48, no. 10, pp. 2685–2693, Oct. 2012

[22] M. Aydin and M. Gulec, "Reduction of cogging torque in double-rotor axial-flux permanent-magnet disk motors: A review of cost-effective magnet-skewing techniques with experimental verification," *IEEE Trans. Ind. Electron.*, vol. 61, no. 9, pp. 5025–5034, Sep. 2014

[23] J. Wanjiku, M. A. Khan, P. S. Barendse, and P. Pillay, "Influence of slot openings and tooth profile on cogging torque in axial-flux PM machines," *IEEE Trans. Ind. Electron.*, vol. 62, no. 12, pp. 7578–7589, Dec. 2015.

[24] A. B. Letelier, D. A. Conzalez, J. A. Tapia, R. Wallace, and M. A. Valenzuela, "Cogging torque reduction in an axial flux PM machine via stator slot displacement and skewing," *IEEE Trans. Ind. Appl.*, vol. 43, no. 3, pp. 685–693, May/Jun. 2007

[25] E. Fornasiero, N. Bianchi, and S. Bolognani, "Slot harmonic impact on rotor losses in fractional-slot permanent-magnet machines," *IEEE Trans. Ind. Electron.*, vol. 59, no. 6, pp. 2557–2564, Jun. 2012

[26] J. Pyrhönen, T. Jokinen, and V. Hrabovcova, *Design of Rotating Electrical Machines*. London, U.K.: Wiley, 2009.

[27] D. Dorrell, M. Popescu, and D. Ionel, "Unbalanced magnetic pull due to asymmetry and low-level static rotor eccentricity in fractional-slot brushless permanent-magnet motors with surface-magnet and consequent-pole rotors," *IEEE Trans. Magn.*, vol. 46, no. 7, pp. 2675–2685, Jul. 2010

[28] J. Li, Z. Liu, and L. Nay, "Effect of radial magnetic forces in permanent magnet motors with rotor eccentricity," *IEEE Trans. Magn.*, vol. 43, no. 6, pp. 2525–2527, Jun. 2007

[29] B. Ebrahimi and J. Faiz, "Diagnosis and performance analysis of three phase permanent magnet synchronous motors with static, dynamic and mixed eccentricity," *IET Electr. Power Appl.*, vol. 4, no. 1, pp. 53–66, Jan. 2010

[30] P. B. Reddy, A. M. El-Refaie, and K.-K. Huh, "Effect of number of layers on performance of fractional-slot concentrated-windings interior permanent magnet machines," *IEEE Trans. Power Electron.*, vol. 30, no. 4, pp. 2205–2218, Apr. 2015

[31] F. Magnussen and C. Sadarangani, "Winding factors and Joule losses of permanent magnet machines with concentrated windings," in *Proc. 2003 IEEE Int. Electr. Mach. Drives Conf.*, Jun. 1–4, 2003, vol. 1, pp. 333–339.

[32] M. Nakano, H. Kometani, and M. Kawamura, "A study on eddy-current losses in rotors of surface permanent-magnet synchronous machines," *IEEE Trans. Ind. Appl.*, vol. 42, no. 2, pp. 429–435, Mar./Apr. 2006.

[33] H. Toliyat, S. Nandi, S. Choi, and H. Meshdin-Kelk, *Electrical Machines: Modeling, Condition Monitoring and Fault Diagnosis*. Boca Raton, FL, USA: CRC Press, 2013.

[34] O. O. Ogidi, P. S. Barendse, and M. A. Khan, "Influence of rotor topologies and cogging torque minimization techniques on axial-flux permanent magnet machine under static eccentricities," in *Proc. 2015 IEEE Energy Convers. Congr. Expo.*, Sep. 20–24, 2015, pp. 1818–1825.

[35] Z.Q. Zhu, "A simple method for measuring cogging torque in permanent magnet machines," in *Proc. 2009 IEEE Power Energy Soc. Gen. Meet.*, Calgary, AB, USA, 2009, pp. 1–4.

[36] G. Heins, M. Thiele, and T. Brown, "Accurate torque ripple measurement for PMSM," *IEEE Trans. Instrum. Meas.*, vol. 60, no. 12, pp. 3868–3874, Dec. 2011.

[37] *DR-2112 In-Line Torque Transducer Data Sheet*, Lorenz Messtechnik Gmbh, Alfdorf, Germany, pp. 1–5, 2010.

[38] J. F. Geiras and M. Wing, *Permanent Magnet Motor Technology, Design and Applications*, 2nd ed. New York, NY, USA: Marcel Dekker, 2002.

Oladapo Omotade Ogidi (M'13) received the B.Sc. degree from the Federal University of Technology, Akure, Nigeria, in 2007, the M.Sc. degree from the University of Benin, Benin City, Nigeria, in 2012, and the Ph.D. degree from the University of Cape Town, Cape Town, South Africa, in 2016.

He is currently an Electrical Power Engineer with Suzlon Energy Limited, Rostock, Germany, where he is involved in the development of wind generator technologies. His research interests include electrical machine design, condition monitoring, and wind energy conversion system.

Paul S. Barendse (M'07) received the B.Sc., M.Sc., and Ph.D. degrees in electrical engineering from the University of Cape Town, Cape Town, South Africa, in 2001, 2005, and 2007, respectively.

In 2002, he was with the mining company IMPLATS, where he fulfilled the role as a Junior Engineer. He is currently in the Department of Electrical Engineering, University of Cape Town, where he is an Associate Professor. He specializes in the areas of power electronics, drives, and machines. His research focuses on signal processing techniques applied to power applications.

Mohamed Azeem Khan (M'07–SM'13) received the B.Sc., M.Sc., and Ph.D. degrees in electrical engineering from the University of Cape Town, Cape Town, South Africa, in 1994, 2001, and 2006, respectively.

He was with Koeberg Nuclear Power Station in South Africa as a Maintenance Engineer and System Engineer on the turbine and generator control systems. He also spent two years with Clarkson University, NY, USA, where he taught a semester course in energy conversion and worked on several research projects for NYSERDA and several companies including Warner Energy and Advanced Machines and Drives. He is currently in the Department of Electrical Engineering, University of Cape Town, where he is an Associate Professor. His research interests include permanent-magnet machine design and control of renewable energy systems.